Suppressing the excitonic effect and reducing the overpotential in narrow band gap covalent organic frameworks of Lieb lattice to enable metal-free photocatalytic overall water splitting

Hongde Yu[1] and Dong Wang[1*]

[1]MOE Key Laboratory of Organic OptoElectronics and Molecular Engineering, Department of Chemistry, Tsinghua University, Beijing 100084, P. R. China
[*]**Corresponding author. Email: dong913@mail.tsinghua.edu.cn**

Abstract

Two-dimensional (2D) layered covalent organic frameworks (COFs) with in-plane conjugation and out-of-plane π-stacked structures have emerged as promising organic photocatalysts for their highly designable skeleton, tunable electronic properties, and inherent pores. Currently, wide band gap COFs are often applied for photocatalytic water splitting to surpass the large kinetic barrier of chemical reactions, which is adverse to solar light harvest and seriously impedes the promotion of energy conversion efficiency. In this work, we propose to exploit narrow band gap COFs as photocatalysts and devote to reduce the overpotential of redox reactions by engineering active catalytic sites on them. By first-principles calculations, we design nine fully conjugated COFs of Lieb lattice with band gaps tunable from 1.72 eV to 1.00 eV, which show broad visible and near-infrared (NIR) light absorption. Further, we unravel that the enhanced optical absorption is accompanied by the suppressed excitonic effect because the narrowed band gap has produced increased dielectric screening within the electron-hole pair. Interestingly, a pre-designed hydrogen bond can significantly reduce the overpotential of hydrogen evolution reaction, solving the dilemma of insufficient driving force posed by the narrow band gap. Finally, we demonstrate that a tandem system based on two of our designed COFs are capable of metal-free overall water splitting under visible and NIR light. Our findings highlight a new route to realize metal-free photocatalysis with COFs and pave the way for the rational design of organic photocatalysts with high energy conversion efficiency.

Introduction

Photocatalytic water splitting utilizes inexhaustible sunlight and earth-abundant water for hydrogen production, and has becomes one of clean and sustainable solutions to the global energy crisis.[1-4] Since the first demonstration of TiO_2 photoanode and Pt counter electrode for water oxidation and reduction in 1970s,[5] solar-to-hdyrogen energy conversion has attracted tremendous attention.[6-7] Inspired by natural photosynthesis, organic conjugated materials with tunable electronic structures, as represented by *g*-C_3N_4,[8-9] conjugated microporous polymers (CMPs),[10] linear conjugated polymers,[11-13] two-dimensional (2D) polymers,[14-15] and covalent organic frameworks (COFs),[16-23] are emerging as novel photocatalysts. COFs are a class of

porous materials which integrate molecular building blocks into periodic skeleton via reticular chemical reactions,[24-25] their high crystallinity, tunable pore size, large specific surface area, and high chemical and thermal stability make them promising photocatalyts.[26-28] 2D layered COFs with impressive hydrogen evolution activities have been reported lately, such as azine-linked N_3-COF and cyano-vinylene-linked sp^2c-COF demonstrating hydrogen evolution rate of 1.7 mmol g^{-1} h^{-1} and 1.36 mmol g^{-1} h^{-1}, respectively, and functionalization with electron withdrawing end groups of the latter further increased the rate to 2.12 mmol g^{-1} h^{-1}.[17, 21] Despite the rapid experimental progress,[29-32] very few works reported the solar-to-hydrogen (STH) energy conversion efficiency of above 1%,[9] so designing new COFs with superior photoelectrochemical performance based on the rational regulation of a series of inter-related and contradictory factors in a photocatalytic process is highly demanded.

One major challenge faced is the overwhelmingly high energy barrier of reactions on non-metal photocatalysts,[33-34] here COFs, which in turn causes the large overpotential (η) in the solar energy conversion. More specifically, in order to surpass the energy barrier associated with the reaction kinetics, ultraviolet light is often uptaken so that the photoexcited electron and hole can be supplied with sufficient energy (U) to trigger the chemical transformation. That's why COFs with large band gaps (E_g) above 2.5 eV have been applied for photocatalytic water splitting, such as N_3-COF with E_g of 2.6-2.7 eV.[17] It, however, will lead to the inefficient harvest of visible and near-infrared (NIR) light, which accounts for over 80% of the solar power.[35] In view of this, it is of great promise to design new COFs with lower overpotential and smaller band gap below 2.0 eV to enable visible-to-NIR light-driven water splitting. The other challenge arises from the strong excitonic effect in organic photocatalysts. The photoexcited electron-hole pair, namely the exciton, is strongly bounded in COFs due to the large reduced mass (m^*) of exciton and the small dielectric constant (ε_s), which will foster undesirable charge recombination and therefore drop the internal quantum efficiency.[36] So, in order to suppress the excitonic effect we must increase the dielectric screening. Qualitatively, the smaller band gap implies stronger screening and weaker binding of the electron-hole pair. A linear scaling law between the exciton binding energy (E_b) and the band gap has been established in 2D materials.[37-38] Although the scaling law in COFs remains to be discovered, we foresee a promising way to regulate the excitonic effect by engineering the band gap.

In this work, we explore the fundamental structure-property relationship of COFs as organic photocatalysts and propose an effective approach to regulate key photoelectrochemical properties of COFs, i.e., the band gap E_g, the exciton binding energy E_b, the overpotential η, and the driving force U, to achieve metal-free overall water splitting. Their inter-relations are sketched in **Fig. 1**. We design nine fully conjugated COFs of Lieb lattice with pyrene as node and cyano-vinylene as linkage, which are experimentally available via the Knoevenagel reaction. By edge building block modifications, the band gap of COFs is effectively tuned from 1.72 eV to 1.00 eV to absorb the visible and NIR light. With the state-of-the-art *GW*-BSE method, we have, for the first time, established a linear scaling law between the electronic dielectric

constant and the inverse square of optical band gap of 2D layered COFs. More importantly, we solve the dilemma of insufficient driving force posed by the narrow band gap by reducing the overpotential in photocatalytic reactions, and find that introducing hydrogen bond to stabilize the reaction intermediate is an effective approach to reduce the overpotential. Based on these discoveries, we demonstrate that combining two of our newly designed COFs in a tandem cell is capable of metal-free overall water splitting with a theoretical STH efficiency of over 30%. The structure-property-activity relationships disclosed herein not only shed light on the rational design of new COFs with desired water splitting activity, but also tremendously boost their applications in other photocatalytic chemical transformations.[39-40]

Results

COFs of Lieb lattice are constructed by node units of C_2 or C_4 symmetry with four arms and linear edge units with two arms, whereas COFs of kagome lattice are built merely by node units of C_3 symmetry. Comparing to COFs of kagome or honeycomb-kagome lattice with flat band around the Fermi level such as N_3-COF, COFs of Lieb lattice usually possess dispersive bands at VBM and CBM (**Fig. S1** and **S2**) resulting in smaller effective mass of electron and hole.[41] Therefore, COFs of Lieb lattice have been widely explored as emerging organic semiconductors with high mobility in the experiment.[42] On the other hand, different from COFs of kagome or honeycomb-kagome lattice built with only one component, such as N_3-COF whose band gap is only determined by its node unit, COFs of Lieb lattice are composed of two types of building blocks, node and edge. This structural construction provides a large chemical space to tune their electronic properties, especially the band gap and band edge energies by the molecular design method, and opportunities to explore the fundamental structure-property relationship. Many COFs of kagome lattice possess large band gaps, for example, 2.6-2.7 eV for N_x-COFs (x = 0-3),[17] 2.8 eV for TFPT-COF,[43] and 4.0 eV for COF-5.[25] Recently, sp^2c-COF, a COF of Lieb lattice with the band gap of 2.03 eV, has been demonstrated as novel photocatalysts for visible-light-driven hydrogen production.[44] However, it remains yet unknown whether the absorption band edge of such COFs can be further shifted into the NIR region and more importantly, how to achieve metal-free photocatalysis for overall water splitting with them.

In order to attain suitable band gaps and optimal band edge positions for the visible-to-NIR-light-driven overall water splitting, we have designed nine fully conjugated COFs of Lieb lattice with a pyrene node, a cyano-vinylene linkage and various edge units, and their layer-stacked structures are intrinsically different from 2D polymers. These COFs are denoted as PPy-Ph, PPy-BT, PPy-BT(F), PPy-PT, PPy-PT(F), PPy-TDQ, PPy-TzBI, PPy-Q, and PPy-Q(F), respectively as sketched in **Fig. 1**. Herein, PPy represents the pyrene node and it is short for tetrakis(4-formylphenyl)phenyl; Ph, BT, PT, TDQ, TzBI, and Q represent the edges, which are short for phenyl, benzothiadiazole, pyridal[2,1,3]thiadiazole, thiadiazoloquinoxaline, pyrrolo[3,4-f]benzotriazole-5,7-dione, and quinoxaline; F

represents peripheral fluorine substitution.

PPy-Ph is the so-called sp^2c-COF composed of the PPy node and the Ph edge, linked by cyano-vinylene to form fully π-conjugated structure. As reported by Jiang and co-workers,[21] it exhibited highly active hydrogen production of about 2.1 mmol h^{-1} g^{-1} under the visible light irradiation in the presence of triethanolamine (TEOA) sacrificial agent and Pt co-catalyst. PPy-Ph is a semiconductor with the indirect band gap of 1.72 eV (**Fig. 2A** and **Fig. 3A** calculated by the HSE06 method), consistent with the experimental result of 1.9 eV.[21] As illustrated by the partial density of states (pDOS) in **Fig. 3A**, both CBM and VBM in PPy-Ph are essentially comprised by C-$2p_z$ orbitals, confirming the formation of extended π-conjugation. Further, the charge density at VBM is mainly localized on the pyrene node, while that at CBM is delocalized over both node and edge (**Fig. 3B**). From a molecular perspective, HOMO of the PPy node is far higher than that of the Ph edge while LUMO of PPy is slightly lower than Ph, as illustrated by the energy level alignment of building blocks in **Fig. 2B**. As for band edge energies, VBM and CBM in PPy-Ph relative to the vacuum level are -5.24 eV and -3.52 eV, indicating its capability of photocatalytic HER at pH = 7 whereas prohibited OER (**Fig. 2A**). Our results are consistent with the observed superior HER activity (2.1 mmol g^{-1} h^{-1}) and very small OER rate (0.022 mmol g^{-1} h^{-1}) of sp^2c-COF.[21]

In contrast to PPy-Ph, COFs composed of edges whose LUMO is deeper possess smaller band gaps (**Fig. 2A**). Taking PPy-BT as an example, it is a semiconductor with the indirect band gap of 1.57 eV, smaller than PPy-Ph of 1.72 eV. As illustrated by the charge density distribution of PPy-BT in **Fig. S3**, its VBM is dominantly contributed by the PPy node while CBM is mainly localized on the BT edge. From the perspective of molecular building blocks, the reduced band gap in PPy-BT can be attributed to the fact that LUMO of the BT edge is much lower than that of the PPy node (**Fig. 2B**). Besides, the energies of VBM and CBM in PPy-BT are -5.28 eV and -3.71 eV, indicating its capability of photocatalytic water splitting at pH = 7, especially for HER (**Fig. 2A**). Further, we find that PPy-BT(F) with electron-withdrawing F-substitution have increased the driving force for OER at pH = 7, as indicated by the lower VBM energy of -5.33 eV in PPy-BT(F) (**Fig. 2A**). These results imply that PPy-BT(F) is capable of overall water splitting. Such simultaneous decrease of VBM and CBM energies is ascribed to the F-substitution with strong electron-withdrawing effect, which lowers both HOMO and LUMO energies of the BT edge. The F-substitution effect is also observed in other COFs such as PPy-PT(F) and PPy-Q(F). This functional group modification strategy provides a simple yet effective approach to tune the band edge energies of COFs towards overall water splitting, and it also modifies the microenvironment of pore surfaces.[45]

Furthermore, we demonstrate a positive correlation between LUMO energies of edges and band gaps of COFs (**Fig. 2A**, **Fig. 2B**, and **Table S1**). In addition to PPy-BT and PPy-BT(F) mentioned above, all other COFs designed possess smaller band gaps than PPy-Ph (**Table 1**, **Fig. 2A**, **Fig. S3-S15** and **Table S2**). Among them, PPy-TDQ has the smallest band gap of 1.00 eV ascribed to the low-lying LUMO of the TDQ edge

and its strong electron-accepting ability. The narrowed band gap in turn gives rise to the red-shifted absorption spectroscopy. PPy-Ph exhibits broad absorption in the range of 300 to 650 nm covering the visible region of the solar spectrum and peaks at ~ 500 nm as calculated by the G_0W_0-BSE method (**Fig. 2C**). Our results are in good agreement with the experimental absorption spectrum of PPy-Ph which spans from 360 to 620 nm with a maximum absorption at 497 nm, and the calculated optical band gap of 2.14 eV also corresponds well with the experimental value of 2.03 eV.[21] In comparison, the absorption spectra of other COFs are further broadened and extend to 900 nm when the LUMO of edges becomes deeper and deeper (**Fig. 2C** and **Fig. S17**). Among them, PPy-TDQ shows the broadest absorption spanning from 300 to 900 nm and can harvest a wide range of visible and NIR light. These results demonstrate superior light harvesting ability of newly designed COFs to the well-known *g*-C_3N_4 and N_3-COF with larger band gap of 2.7 eV[17, 46] and absorption below 400 nm and 500 nm, respectively, which covers only a small portion of the visible region.

As for band edge positions, we see good correlations between VBM and CBM energies of COFs and HOMO and LUMO energies of edge units, indicating that band edge energies can be effectively modulated by edge units to straddle the electrical potentials of HER and OER. According to **Fig. 2A**, all these COFs can trigger HER under standard conditions (pH = 0). In neutral solution (pH = 7), five of them, namely PPy-BT, PPy-BT(F), PPy-TzBI, PPy-Q, and PPy-Q(F), can serve as photocatalysts for overall water splitting, while PPy-PT and PPy-PT(F) are designed for OER. For those COFs that only activate half-reactions in photocatalytic water splitting, electron donating or accepting sacrificial agents like TEOA or $AgNO_3$ are required.[21] An alternative solution is combining these COFs to form a Z-scheme heterostructure where a high energy conversion efficiency has also been observed.[9, 47]

It is worth mentioning that all these designed COFs are constructed by node and edge building blocks linked by cyano-vinylene and share the same Lieb lattice as sp^2c-COF, so they can be synthesized via the Knoevenagel polycondensation reaction with chemicals commonly used to fabricate organic photovoltaic polymers, as summarized in **Fig. S18**.[31, 39, 48] The fully conjugated structure of cyano-vinylene-linked COFs also benefits the exciton dissociation and charge transport to avoid undesirable recombination and annihilation, which distinguishes them from non-conjugated linkages such as boronic ester and boronate. Besides, the polar cyano group in this linkage has increased the hydrophilicity of pore wall surfaces, which is proved to be essential for photocatalytic hydrogen evolution from water, especially with metal-free photocatalysts.[49]

2.2 Suppressing the excitonic effect to promote the electron-hole separation

Following the photon absorption, the Coulombic bound electron-hole pair, namely the exciton, is generated and subsequently dissociates into free charge carriers to trigger electrochemical reactions at the interface. The exciton binding energy is a key measure of the electrostatic interaction within an electron-hole pair. It can be defined as E_b =

E_{elec} - E_{opt},[50] where E_{elec} is the quasiparticle electrical band gap corresponding to the lower bound of inter-band transition, while E_{opt} represents the optical band gap derived from the absorption spectroscopy.[51] Although the strong excitonic effect in organic photocatalysts has been well recognized,[29] how to accelerate the exciton dissociation remains an open question. In principle, the exciton binding energy is determined by the reduced mass (m^*) of exciton and the dielectric screening (ε_s).[51] Herein, we address the issue of strong excitonic effect in COFs by decreasing the mass of exciton m^* with topological design and increasing the static dielectric constant ε_s via chemical structure design.

When node units of C_3 symmetry are used to construct COFs of kagome lattice, a flat band typically shows up at CBM or VBM.[41, 52] This flat band is formed by non-bonding orbitals and associated with heavy electron or hole, which can lead to intriguing magnetic phenomenon but is not desired for high-mobility charge transport.[41] Since the reduced mass of exciton is defined as $1/m^*=1/m_e^*+1/m_h^*$,[51] where m_e^* and m_h^* stand for the effective mass of electron and hole, respectively, the flat band at CBM or VBM can give rise to relatively large reduced mass of exciton and in turn strong binding of the electron-hole pair. In contrast, COFs constructed by node units of C_2 or C_4 symmetry, such as PPy, porphyrin, and phthalocyanine, form Lieb lattice.[41] In COFs of Lieb lattice, both valence and conduction bands are dispersive formed by bonding/antibonding orbitals, which leads to small effective mass of electron, hole, and exciton.

The static dielectric constant measures the Coulombic screening effect in a solid lattice. The increased static dielectric constant implies the decreased binding of electron-hole pair. In organic solids, the static dielectric constant usually falls between 3-4, which is much smaller than inorganic crystals such as photovoltaic perovskite materials.[53] In low-frequency or static electric fields, dielectric response arises from both ionic and electronic contributions, and it can be written as $\varepsilon_s = \varepsilon_{s,ion} + \varepsilon_{s,elec}$.[54] The ionic response ($\varepsilon_{s,\ ion}$) is associated with the motion of atoms which can generate oscillating dipole as with infrared active lattice vibrations and is of particular importance to inorganic solids. The electronic response ($\varepsilon_{s,elec}$) accounts for the change of electronic polarizability with the electric field, and it is the dominating mechanism for organic solids, especially nonpolar materials. According to the Lorentz oscillator model, the electronic static dielectric ($\varepsilon_{s,elec}$) can be related to the optical absorption frequency (ω_e) by $\varepsilon_{s,\ elec} = 1 + Ne^2/(m\varepsilon_0\omega_e^2)$, where m and N are the mass and number of oscillators per volume, respectively, and ω_e represents the resonance frequency of oscillation corresponding to the average electronic excitation energy.[54] So, when the optical band gap is narrowed the static dielectric constant will increase, leading to more effective electrostatic screening and weaker binding of the electron-hole pair.

As illustrated in **Fig. 4A** and **Fig. S19**, we find a linear relationship between the electronic static dielectric $\varepsilon_{s,elec}$ and E^{-2}_{opt} which is consistent with the Lorentz oscillator model. This implies that the dielectric screening can be increased by reducing the optical band gap. Correspondingly, the exciton binding energy E_b calculated by the

G_0W_0-BSE method, a state-of-the-art approach to account for the excitonic effect, is substantially reduced when the optical absorption is red-shifted to the NIR region in all the designed COFs of Lieb lattice, as shown in **Fig. 4B**. We notice that the reduced mass of exciton barely changes in these COFs as indicated by **Table S2**. The determination of E_b by ε_s of 2D layered COFs is very different from that of 3D inorganic semiconductors, where the screening effect is very large and the effective mass m^* becomes the dominating factor of E_b, and it also differs from 2D semiconductors where a linear scaling law between E_b and the quasiparticle band gap E_{elec} with $E_b \approx E_{elec}/4$ was established.[38] Specifically, the experimentally synthesized sp^2c-COF (PPy-Ph) has the exciton binding energy of about 1200 meV, which is comparable to *g*-C_3N_4 of 1200 meV,[46] while all the newly designed COFs have smaller exciton binding energy. In particular, PPy-TDQ exhibits E_b of 700 meV, nearly half that of sp^2c-COF and *g*-C_3N_4, which can be attributed to its relatively large dielectric constant of 6.05 (**Table 1**). So far, we have demonstrated that enhanced solar-light absorption and prompt exciton dissociation are simultaneously realized in narrow band gap COFs.

All these COFs, except for PPy-PT, PPy-PT(F), and PPy-Q, possess an indirect band gap where VBM and CBM appear at different k-points, so the photo-generated electron and hole have different momenta. Accordingly, a transition from CBM to VBM will require change of the electron wavevector, which can inhibit the exciton annihilation and prolong its lifetime,[54] different from COFs of kagome lattice with a direct band gap. On the other hand, as illustrated by the partial charge density distribution in **Fig. 3D** and **Fig. S4-S16**, VBM in all COFs, except for PPy-Ph, arises primarily from the node and CBM from the edge, owing to the large energy offset between both HOMO and LUMO of node and edge units. Such a feature indicates that the photo-generated electron-hole pair is spatially separated, which favors the exciton dissociation, similar to that in type-II heterostructures with a staggered band gap. Furthermore, node and edge units stack in the out-of-plane direction forming a one-dimensional channel for hole and electron transport, respectively. These divided transport channels represent a unique character of 2D layered COFs, which can enlarge the interface area of electron and hole and boost their separation (**Fig. 4C**). In addition, the inherent pores in 2D layered COFs provide a favorable environment for chemical reactions so that the migration distance of charge carriers can be shortened, while the large surface area also provides adequate space for the high-load of co-catalyst as well as opportunities to engineer active sites on them to achieve metal-free catalysis (**Fig. S20-S21**).

2.3 Reducing the overpotential via intramolecular hydrogen bond to enable metal-free water splitting with high STH efficiency.

After the photo-generated exciton dissociate into electron and hole, these free charge carriers will trigger the redox reactions at the interface of electrolyte and COFs. To enable hydrogen production, CBM in COFs must be sufficiently higher than the reduction potential of water, namely -4.03 eV (vs. vacuum) in neutral solution (pH = 7) or -4.44 eV at pH = 0, so that adequate driving force (U) can be supplied to the electron

to overcome the energy barriers associated with HER.[55] However, high CBM often implies wide band gap and may cause blue-shift of the absorption spectroscopy, which is adverse to efficient sunlight harvesting. To apply narrow band gap COFs for metal-free HER, we need to engineer pore walls of COFs and create active catalytic sites with low overpotential to boost their hydrogen evolution rate. In contrast to inorganic metal co-catalysts with partially filled d- or f- orbitals, such as Pt and $Co(NO_3)_2$, metal-free catalysts with low overpotential are not readily attainable, and design of active sites on organic photocatalysts has attracted increasing attention, especially for HER.[8] A recent work showed that the nitrogen-site on the linkage of 2D polymers of kagome lattice, such as imine, azine, and azo groups, could serve as active catalytic site for metal-free HER.[55] To reduce the overpotential, it is essential to reduce the hydrogen adsorption free energy by stabilizing the reaction intermediate H*. However, except for highly reactive organic radicals with unpaired electrons, adsorption of hydrogen on a closed-shell organic compound has to break a chemical bond and produces an unstable radical intermediate. This process is usually associated with highly positive Gibbs free energy change ΔG(H*) and large overpotential (η). Therefore, novel principles to delicately design the chemical structure of reaction intermediates on COFs are demanded.

By calculating the Gibbs free energy change of hydrogen adsorption ΔG(H*) on designed cyano-vinylene-linked COFs,[56] we propose to engineer active sites on a weak chemical bond and stabilize H* by non-covalent intramolecular interactions such as hydrogen bond. We take PPy-BT as an example to illustrate the catalytic activity of newly designed COFs. As shown above, the photo-generated electron at CBM in all these COFs is mainly localized on the edge unit. So, we investigate the Gibbs free energy change of HER for all the potential catalytic sites on the BT edge under the standard condition (**Fig. 5A**). The overall trend of ΔG(H*) is S > C > N while the local environment also significantly influences the value. We notice that hydrogen adsorption on the sulfur-site is energetically most unfavorable because a sulfur atom tends to form two σ bonds and it is already saturated in COFs. The carbon-site on the cyano-group (-CN) attached to the vinylene linkage also shows relatively high ΔG(H*) because hydrogen adsorption on it needs to break the strong C≡N bond. However, the carbon-site on the BT edge possesses moderate ΔG(H*), since adsorption of a hydrogen atom on the aromatic carbon will break the weak π bond and change its hybridization from sp^2 to sp^3. The N2 site on the BT edge shows the smallest ΔG(H*) of 0.26 eV, which we attribute to the formation of an intramolecular hydrogen bond with the nearby nitrogen atom on the cyano-group that has stabilized the H* intermediate (**Fig. 5B**). While on the N1 site of the same BT edge, ΔG(H*) is larger due to the absence of hydrogen bond interaction. These results manifest that the overpotential in HER can be substantially reduced by introducing intramolecular hydrogen bond interaction, and the active catalytic site is attainable in designed cyano-vinylene-linked COFs with hetero-nitrogen-atom on the edge.

In contrast, ΔG(H*) is 0.72 eV for PPy-Ph (sp^2c-COF) due to lack of active nitrogen site, so metal-free HER with low-energy excitons is prohibited on it (**Fig. S22**).

We should point out that the cyano-group participating in the hydrogen bond formation can be introduced to COFs in the synthesis via the Knoevenagel polycondensation reaction,[21, 57-58] so it exists in all the newly designed COFs here and we have observed reduced overpotential due to the hydrogen bond interaction in all of them (**Fig. 5D** and **Fig. S23-S28**). And similar tendency of ΔG(H*), namely S > C > N, has been found in COFs other than PPy-BT (**Fig. 5C**), while the hydrogen-bond-assisted overpotential reduction mechanism has been verified for all the designed COFs (**Fig. 5D**). Therefore, introducing nitrogen-rich sites to the edge of COFs and establishing hydrogen bond interaction in H* are a promising strategy to achieve metal-free hydrogen evolution, and this method also applies to other organic photocatalysts, including linear conjugated polymers and CMPs.

In order to further validate that the photo-generated electron can indeed drive the water reduction reaction in neutral solution (pH = 7), we calculate the Gibbs free energy change on the N2 site, the active nitrogen site of PPy-BT in the presence and absence of light-induced bias potential (*U*), respectively. As shown in **Fig. 5E**, in the dark this bias potential is equal to zero and each fundamental step of the reaction is up-hill in energy so it is thermodynamically forbidden. However, under the visible light irradiation the bias potential is 0.73 eV and the reaction turns down-hill, which implies that the N2 site of PPy-BT is capable of metal-free photocatalytic HER in neutral solution. Interestingly, we notice that adsorption of a hydrogen atom on the N2 site can also reduce the overpotential of nearby sites on the same edge unit, such as C, S, and N1 sites, and it even turns the nearby N1 site into an active catalytic site, which would immensely accelerate the hydrogen production reaction (**Fig. 5F** and **Fig. S29**). This phenomenon can be understood from the formation of stable closed-shell intermediate after two hydrogen atoms are simultaneously adsorbed onto COFs, and it is consistent with previous observation of reduced overpotential at high hydrogen coverage.[56] Altogether four of our designed COFs show promising metal-free photocatalytic activity for HER in neutral solution (pH = 7) under visible light irradiation, and they are PPy-BT, PPy-BT(F), PPy-TzBI, and PPy-Q.

Finally, we demonstrate that metal-free overall water splitting with these designed narrow band gap COFs is feasible, by constructing a direct Z-scheme heterojunction to harvest visible-to-NIR light and simultaneously provide adequate driving force for both HER and OER, as illustrated in **Fig. 6A**. In this system, PPy-BT and PPy-TDQ serve as metal-free photocatalysts for HER in neutral solution of pH = 7 and 0.1 M ascorbic acid solution of pH = 2.6, respectively (**Fig. 5E** and **Fig. 6B**), while PyTz-Ph is designed as the photocatalyst for OER (**Fig. 6C** and **Fig. 6D**). Here PyTz is short for 3,3',3",3'"-(1,9-dihydropyrene-1,3,6,8-tetrayl)tetrakis(1,2,4,5-tetrazine), and it is used to replace the PPy node in PPy-Ph to form PyTz-Ph. The tetrazine modification of pyrene has substantially lowered the VBM and CBM of PyTz-Ph, making it capable of OER. The HER takes place on the BT or TDQ edge unit whereas the OER mainly occurs on the PyTz node unit, which is different from OER taking place on the Ph unit in other 2D polymers.[34] Meanwhile, PyTz-Ph and PPy-BT possess small band gaps of 1.50 eV and 1.57 eV, respectively that can absorb visible light below 700 nm, while the

band gap of PPy-TDQ is down to 1.00 eV which can absorb both visible and NIR light below 900 nm. Furthermore, such a tendem system is flexible and also applicable to other pH conditions by combining narrow band gap COFs with suitable band edge positions. As illustrated in **Fig. 6C** and **Fig. 6D**, PyTz-Ph can serve as photocatalyst for metal-free OER under visible-to-NIR light irradiation at both pH = 2.6 and pH = 7 in 0.1 M ascorbic acid solution and neutral solution, respectively. Both solutions are commonly used and have been proved effective in photocatalytic experiments of COFs. [49] Actually, PyTz-Ph can be used as photoanode under both acidic and alkaline conditions, and all the eight aforementioned COFs can be employed as photocathode in various solutions, and further combined with PyTz-Ph to achieve overall water splitting with high STH efficiency. Among them, PPy-TDQ can reach the highest STH efficiency of about 56.6% in ascorbic acid solution, while PPy-BT is suitable for HER in neutral solution with a theoretical STH efficiency of about 32.8%.

Discussion

In conclusion, we have presented a practical route to regulate the excitonic effect in organic photocatalysts and addressed the dilemma in metal-free photocatalysis, which is whether to increase the band gap to provide enough driving force for chemical reactions or to decrease the band gap to enhance solar light harvest, in order to facilitate overall water splitting with a high STH efficiency. In contrast to previous scenarios that apply wide band gap COFs as photocatalysts, our solution is to design narrow band gap COFs to harvest visible and NIR solar light and at the same time reduce the overpotential of reaction. We propose nine fully conjugated COFs of Lieb lattice with the pyrene node, cyano-vinylene-linkage, and electron-accepting edge units, which possess tunable band gaps ranging from 1.72 to 1.00 eV, with broad harvest of sunlight in visible and NIR regions. Their VBM and CBM energies are also effectively tuned to match the redox potential of water in both acidic and alkaline solutions by edge unit engineering and functional group modifications. By employing the advanced *GW*-BSE approach, we for the first time establish a linear scaling relation between $\varepsilon_{s,\,elec}$ and E_{opt}^{-2} in COFs, which implies that narrowing the band gap can increase the dielectric constant and suppress the pronounced excitonic effect in organic semiconductors. Among these COFs, PPy-TDQ has the broadest light adsorption below 900 nm, the smallest band gap of 1.00 eV and exciton binding energy of 700 meV, which is nearly half of that in *g*-C_3N_4. By scrutinizing active catalytic sites on COFs, we demonstrate that it is feasible to enhance light absorption and simultaneously provide sufficient driving force for photocatalytic water splitting. We unravel a general trend of the overpotential on various catalytic sites of COFs, which is N < C < S, and the vital role of hydrogen bond, inherently associated with the –CN group in these cyano-vinylene-linked COFs, in stabilizing the intermediates and decreasing the overpotential of photocatalytic reactions, especially for HER. Based on these discoveries, we propose a tandem system that combines two COFs of Lieb lattice as photoanode and photocathode respectively for overall water splitting under visible and NIR light irradiation. This system is flexible and highly extensible to a large variety of COFs to enable overall water splitting in solutions of a broad range of pH, while a very high theoretical STH

efficiency can be reached, such as 56.6% for PPy-TDQ and 32.8% for PPy-BT. Our work not only provides a practical strategy to regulate the excitonic effect and the overpotential in COFs for visible-to-NIR-light-driven water splitting, but also sheds light on developing novel metal-free photocatalysts for other chemical transformations.

Materials and Methods

We performed density functional theory (DFT) calculations for all the electronic properties of COFs in this work, including the optimization of lattice constants and atomic coordinates, as implemented in the Vienna ab-initio simulation package (VASP 5.3.5)[59] using the projector augmented wave (PAW)[60] method and Perdew−Burke−Ernzerhof (PBE)[61] exchange-correlation functional. Grimme's D3 approach was applied to include the London dispersion correction,[62] and Heyd−Scuseria−Ernzerhof (HSE06)[63] hybrid functional was used to calculate the accurate band gap of COFs. Coordinates of high-symmetry k-points in band structures were provided in **Table S3**. The electronic and ionic dielectric constants were calculated with linear response theory and density functional perturbation theory (DFPT) implemented in VASP 5.3. Further, the *GW* method at the level of G_0W_0 was applied to calculate the quasiparticle band gap and it was combined with the Bethe−Salpeter equation (BSE) to obtain the optical band gap and exciton binding energy. In the lattice parameter optimization, a cut-off energy of 400 eV for the plane-wave basis set was employed while in the static calculations a cut-off energy of 600 eV was used. And the convergence criterion of forces during the atomic optimization was 0.02 eV $Å^{-1}$. The energy convergence criterion in the self-consistent field iteration was 10^{-5} eV in the optimizations while 10^{-6} eV in the static calculations. The k-mesh of 1×1×5 was used in the structural relaxation of COFs while denser k-mesh of 1×1×8 was used to obtain the converged charge density. To model the hydrogen evolution reaction, a 1×1×3 supercell of COFs was constructed, and the hydrogen atom was adsorbed to different sites on the edge unit. A k-mesh of 1×1×3 was used to optimize the structure of H^*. Computational hydrogen electrode model was applied and Gibbs free energies were derived using the approach proposed by Nørskov.[56] The spin-polarization effect was considered in the calculation of hydrogen-adsorbed intermediate H^*. The long-range corrected functional ωB97XD and the def2tzvp basis set were used to calculate the frontier orbital energies of molecular building blocks of COFs with the *Gaussian16* program package.[64]

References

1. T. Hisatomi; K. Domen, Reaction systems for solar hydrogen production via water splitting with particulate semiconductor photocatalysts. *Nat. Catal.* **2**, 387-399 (2019).

2. A. Kudo; Y. Miseki, Heterogeneous photocatalyst materials for water splitting. *Chem. Soc. Rev.* **38**, 253-278 (2009).

3. Y. Wang; H. Suzuki; J. Xie; O. Tomita; D. J. Martin; M. Higashi; D. Kong; R. Abe; J. Tang, Mimicking natural photosynthesis: Solar to renewable H_2 fuel synthesis by Z-scheme water splitting systems. *Chem. Rev.* **118**, 5201-5241 (2018).

4. K. Sivula; R. van de Krol, Semiconducting materials for photoelectrochemical energy conversion. *Nat. Rev. Mater.* **1**, 15010 (2016).

5. A. Fujishima; K. Honda, Electrochemical photolysis of water at a semiconductor electrode. *Nature* **238**, 37-38 (1972).

6. S. Chen; T. Takata; K. Domen, Particulate photocatalysts for overall water splitting. *Nat. Rev. Mater.* **2**, 17050 (2017).

7. Q. Wang; T. Hisatomi; Q. Jia; H. Tokudome; M. Zhong; C. Wang; Z. Pan; T. Takata; M. Nakabayashi; N. Shibata, et al., Scalable water splitting on particulate photocatalyst sheets with a solar-to-hydrogen energy conversion efficiency exceeding 1%. *Nat. Mater.* **15**, 611-615 (2016).

8. X. Wang; K. Maeda; A. Thomas; K. Takanabe; G. Xin; J. M. Carlsson; K. Domen; M. Antonietti, A metal-free polymeric photocatalyst for hydrogen production from water under visible light. *Nat. Mater.* **8**, 76-80 (2009).

9. D. Zhao; Y. Wang; C.-L. Dong; Y.-C. Huang; J. Chen; F. Xue; S. Shen; L. Guo, Boron-doped nitrogen-deficient carbon nitride-based Z-scheme heterostructures for photocatalytic overall water splitting. *Nat. Energy* **6**, 388-397 (2021).

10. R. S. Sprick; J.-X. Jiang; B. Bonillo; S. Ren; T. Ratvijitvech; P. Guiglion; M. A. Zwijnenburg; D. J. Adams; A. I. Cooper, Tunable organic photocatalysts for visible-light-driven hydrogen evolution. *J. Am. Chem. Soc.* **137**, 3265-3270 (2015).

11. D. J. Woods; R. S. Sprick; C. L. Smith; A. J. Cowan; A. I. Cooper, A solution-processable polymer photocatalyst for hydrogen evolution from water. *Adv. Energy Mater.* **7**, 1700479 (2017).

12. R. S. Sprick; B. Bonillo; R. Clowes; P. Guiglion; N. J. Brownbill; B. J. Slater; F. Blanc; M. A. Zwijnenburg; D. J. Adams; A. I. Cooper, Visible-light-driven hydrogen evolution using planarized conjugated polymer photocatalysts. *Angew. Chem. Int. Ed.* **128**, 1824-1828 (2016).

13. G. Zhang; Z. A. Lan; X. Wang, Conjugated polymers: Catalysts for photocatalytic hydrogen evolution. *Angew. Chem. Int. Edit.* **55**, 15712-15727 (2016).

14. S. Xu; H. Sun; M. Addicoat; B. P. Biswal; F. He; S. Park; S. Paasch; T. Zhang; W. Sheng; E. Brunner, et al., Thiophene ‐ bridged donor–acceptor sp^2-carbon-linked 2d conjugated polymers as photocathodes for water reduction. *Adv. Mater.* **33**, 2006274 (2021).

15. L. Wang; Y. Zhang; L. Chen; H. Xu; Y. Xiong, 2d polymers as emerging materials for photocatalytic overall water splitting. *Adv. Mater.* **30**, 1801955 (2018).

16. J. Thote; H. B. Aiyappa; A. Deshpande; D. Diaz Diaz; S. Kurungot; R. Banerjee, A covalent organic framework-cadmium sulfide hybrid as a prototype photocatalyst for visible-light-driven hydrogen production. *Chem. Eur. J.* **20**, 15961-15965 (2014).

17. V. S. Vyas; F. Haase; L. Stegbauer; G. Savasci; F. Podjaski; C. Ochsenfeld; B. V. Lotsch, A tunable azine covalent organic framework platform for visible light-induced hydrogen generation. *Nat. Commun.* **6**, 8508 (2015).

18. T. Sick; A. G. Hufnagel; J. Kampmann; I. Kondofersky; M. Calik; J. M. Rotter; A. Evans; M. Döblinger; S. Herbert; K. Peters, et al., Oriented films of conjugated 2d covalent organic frameworks as photocathodes for water splitting. *J. Am. Chem. Soc.* **140**, 2085-2092 (2017).

19. T. Banerjee; K. Gottschling; G. k. Savasci; C. Ochsenfeld; B. V. Lotsch, H_2 evolution with covalent organic framework photocatalysts. *ACS Energy Lett.* **3**, 400-409 (2018).

20. X. Wang; L. Chen; S. Y. Chong; M. A. Little; Y. Wu; W.-H. Zhu; R. Clowes; Y. Yan; M. A. Zwijnenburg; R. S. Sprick, et al., Sulfone-containing covalent organic frameworks for photocatalytic hydrogen evolution from water. *Nat. Chem.* **10**, 1180-1189 (2018).

21. E. Jin; Z. Lan; Q. Jiang; K. Geng; G. Li; X. Wang; D. Jiang, 2d sp^2 carbon-conjugated covalent organic frameworks for photocatalytic hydrogen production from water. *Chem* **5**, 1632-1647 (2019).

22. P. Pachfule; A. Acharjya; J. Roeser; T. Langenhahn; M. Schwarze; R. Schomäcker; A. Thomas; J. Schmidt, Diacetylene functionalized covalent organic framework (cof) for photocatalytic hydrogen generation. *J. Am. Chem. Soc.* **140**, 1423-1427 (2018).

23. L. Stegbauer; S. Zech; G. Savasci; T. Banerjee; F. Podjaski; K. Schwinghammer; C. Ochsenfeld; B. V. Lotsch, Tailor-made photoconductive pyrene-based covalent organic frameworks for visible-light driven hydrogen generation. *Adv. Energy Mater.* **8**, 1703278 (2018).

24. P. J. Waller; F. Gándara; O. M. Yaghi, Chemistry of covalent organic frameworks. *Acc. Chem. Res.* **48**, 3053-3063 (2015).

25. A. P. Cote; A. I. Benin; N. W. Ockwig; M. O'Keeffe; A. J. Matzger; O. M. Yaghi, Porous, crystalline, covalent organic frameworks. *Science* **310**, 1166-1170 (2005).

26. X. Li; P. Yadav; K. P. Loh, Function-oriented synthesis of two-dimensional (2d) covalent organic frameworks-from 3d solids to 2d sheets. *Chem. Soc. Rev.* **49**, 4835-4866 (2020).

27. X. Chen; K. Geng; R. Liu; K. T. Tan; Y. Gong; Z. Li; S. Tao; Q. Jiang; D. Jiang, Covalent organic frameworks: Chemical approaches to designer structures and built-in functions. *Angew. Chem. Int. Ed.* **59**, 5050-5091 (2020).

28. N. Huang; P. Wang; D. Jiang, Covalent organic frameworks: A materials platform for structural and functional designs. *Nat. Rev. Mater.* **1**, 16068 (2016).

29. S. Ghosh; A. Nakada; M. A. Springer; T. Kawaguchi; K. Suzuki; H. Kaji; I. Baburin; A. Kuc; T. Heine; H. Suzuki, et al., Identification of prime factors to maximize the photocatalytic hydrogen evolution of covalent organic frameworks. *J. Am. Chem. Soc.*, 9752-9762 (2020).

30. K. Gottschling; G. k. Savasci; H. Vignolo-González; S. Schmidt; P. Mauker; T. Banerjee; P. Rovó; C. Ochsenfeld; B. V. Lotsch, Rational design of covalent cobaloxime-covalent organic framework hybrids for enhanced photocatalytic hydrogen evolution. *J. Am. Chem. Soc.* **142**, 12146-12156 (2020).

31. W. Chen; L. Wang; D. Mo; F. He; Z. Wen; X. Wu; H. Xu; L. Chen, Modulating benzothiadiazole-based covalent organic frameworks via halogenation for enhanced photocatalytic water splitting. *Angew. Chem. Int. Ed.* **59**, 16902-16909 (2020).

32. S. Wei; F. Zhang; W. Zhang; P. Qiang; K. Yu; X. Fu; D. Wu; S. Bi; F. Zhang, Semiconducting 2d triazine-cored covalent organic frameworks with unsubstituted olefin linkages. *J. Am. Chem. Soc.* **141**, 14272-14279 (2019).

33. Y. Jing; Z. Zhou; W. Geng; X. Zhu; T. Heine, 2d honeycomb-kagome polymer tandem as effective metal-free photocatalysts for water splitting. *Adv. Mater.*, 2008645 (2021).

34. Y. Wan; L. Wang; H. Xu; X. Wu; Y. Jinlong, A simple molecular design strategy for two-dimensional covalent organic framework capable of visible-light-driven water splitting. *J. Am. Chem. Soc.* **142**, 4508-4516 (2020).

35. C.-F. Fu; X. Wu; Y. Jinlong, Material design for photocatalytic water splitting from a theoretical perspective. *Adv. Mater.* **30**, 1802106 (2018).

36. H. Wang; S. Jin; X. Zhang; Y. Xie, Excitonic effects in polymeric photocatalysts. *Angew. Chem. Int. Edit.* **132**, 23024-23035 (2020).

37. J.-H. Choi; P. Cui; H. Lan; Z. Zhang, Linear scaling of the exciton binding energy versus the band gap of two-dimensional materials. *Phys. Rev. Lett.* **115**, 066403 (2015).

38. Z. Jiang; Z. Liu; Y. Li; W. Duan, Scaling universality between band gap and exciton binding energy of two-dimensional semiconductors. *Phys. Rev. Lett.* **118**, 266401 (2017).

39. S. Li; L. Li; Y. Li; L. Dai; C. Liu; Y. Liu; J. Li; J. Lv; P. Li; B. Wang, Fully conjugated donor-acceptor covalent organic frameworks for photocatalytic oxidative amine coupling and thioamide cyclization. *ACS Catal.* **10**, 8717-8726 (2020).

40. R. Chen; J. L. Shi; Y. Ma; G. Lin; X. Lang; C. Wang, Designed synthesis of a 2d porphyrin-based sp^2 carbon-conjugated covalent organic framework for heterogeneous photocatalysis. *Angew. Chem. Int. Ed.* **58**, 6430-6434 (2019).

41. S. Thomas; H. Li; C. Zhong; M. Matsumoto; W. R. Dichtel; J.-L. Bredas, Electronic structure of two-dimensional π-conjugated covalent organic frameworks. *Chem. Mat.* **31**, 3051-3065 (2019).

42. M. Wang; M. Wang; H.-H. Lin; M. Ballabio; H. Zhong; M. Bonn; S. Zhou; T. Heine; E. Cánovas; R. Dong, High-mobility semiconducting two-dimensional conjugated covalent organic frameworks with p-type doping. *J. Am. Chem. Soc.*, (2020).

43. L. Stegbauer; K. Schwinghammer; B. V. Lotsch, A hydrazone-based covalent organic framework for photocatalytic hydrogen production. *Chem. Sci.* **5**, 2789-2793 (2014).

44. E. Jin; Z. Lan; Q. Jiang; K. Geng; G. Li; X. Wang; J. Donglin, 2d sp^2 carbon-conjugated covalent organic frameworks for photocatalytic hydrogen production from water. *Chem* **5**, 1632-1647 (2019).

45. A. Nagai; Z. Guo; X. Feng; S. Jin; X. Chen; X. Ding; D. Jiang, Pore surface engineering in covalent organic frameworks. *Nat. Commun.* **2**, 1-8 (2011).

46. W. Wei; T. Jacob, Strong excitonic effects in the optical properties of graphitic carbon nitride g-C_3N_4 from first principles. *Phys. Rev. B* **87**, 085202 (2013).

47. D. J. Martin; P. J. T. Reardon; S. J. Moniz; J. Tang, Visible light-driven pure water splitting by a nature-inspired organic semiconductor-based system. *J. Am. Chem. Soc.* **136**, 12568-12571 (2014).

48. L. Pandey; C. Risko; J. E. Norton; J.-L. Bredas, Donor–acceptor copolymers of relevance for organic photovoltaics: A theoretical investigation of the impact of chemical structure modifications on the electronic and optical properties. *Macromolecules* **45**, 6405-6414 (2012).

49. X. Wang; L. Chen; S. Y. Chong; M. A. Little; Y. Wu; W.-H. Zhu; R. Clowes; Y. Yan; M. A. Zwijnenburg; R. S. Sprick, et al., Sulfone-containing covalent organic frameworks for photocatalytic hydrogen evolution from water. *Nat. Chem.* **10**, 1180-1189 (2018).

50. J.-L. Bredas, Mind the gap! *Mater. Horiz.* **1**, 17-19 (2014).

51. H. Wang; W. Liu; P. Zhang; X. He; X. Zhang; Y. Xie, Toward an excitonic perspective on low-dimensional semiconductors for photocatalysis. *J. Am. Chem. Soc.* **142**, 14007-14022 (2020).

52. M. A. Springer; T.-J. Liu; A. Kuc; T. Heine, Topological two-dimensional polymers. *Chem. Soc. Rev.* **49**, 2007-2019 (2020).

53. N. Cho; C. W. Schlenker; K. M. Knesting; P. Koelsch; H. L. Yip; D. S. Ginger; A. K. Y. Jen, High-dielectric constant side-chain polymers show reduced non-geminate recombination in heterojunction solar cells. *Adv. Energy Mater.* **4**, 1301857 (2014).

54. P. A. Cox, *The electronic structure and chemistry of solids*. Oxford University Press: 1987.

55. Y. Wan; L. Wang; H. Xu; X. Wu; J. Yang, A simple molecular design strategy for two-dimensional covalent organic framework capable of visible-light-driven water splitting. *J. Am. Chem. Soc.* **142**, 4508-4516 (2020).

56. J. K. Nørskov; T. Bligaard; A. Logadottir; J. Kitchin; J. G. Chen; S. Pandelov; U. Stimming, Trends in the exchange current for hydrogen evolution. *Journal of The Electrochemical Society* **152**, J23 (2005).

57. E. Jin; M. Asada; Q. Xu; S. Dalapati; M. A. Addicoat; M. A. Brady; H. Xu; T. Nakamura; T. Heine; Q. Chen, et al., Two-dimensional sp^2 carbon-conjugated covalent organic frameworks. *Science* **357**, 673-676 (2017).

58. X. Zhuang; W. Zhao; F. Zhang; Y. Cao; F. Liu; S. Bi; X. Feng, A two-dimensional conjugated polymer framework with fully sp^2-bonded carbon skeleton. *Polym. Chem.* **7**, 4176-4181 (2016).

59. G. Kresse; J. Furthmüller, Efficient iterative schemes for ab initio total-energy calculations using a plane-wave basis set. *Phys. Rev. B* **54**, 11169 (1996).

60. P. E. Blöchl, Projector augmented-wave method. *Phys. Rev. B* **50**, 17953 (1994).

61. J. P. Perdew; K. Burke; M. Ernzerhof, Generalized gradient approximation made simple. *Phys. Rev. Lett.* **77**, 3865 (1996).

62. S. Grimme; J. Antony; S. Ehrlich; H. Krieg, A consistent and accurate ab initio parametrization of density functional dispersion correction (dft-d) for the 94 elements h-pu. *J. Chem. Phys.* **132**, 154104 (2010).

63. J. Heyd; G. E. Scuseria; M. Ernzerhof, Hybrid functionals based on a screened coulomb potential. *J. Chem. Phys.* **118**, 8207-8215 (2003).

64. M. J. Frisch; G. W. Trucks; H. B. Schlegel; G. E. Scuseria; M. A. Robb; J. R. Cheeseman; G. Scalmani; V. Barone; G. A. Petersson; H. Nakatsuji, et al. *Gaussian 16 rev. C.01*, Wallingford, CT, 2016.

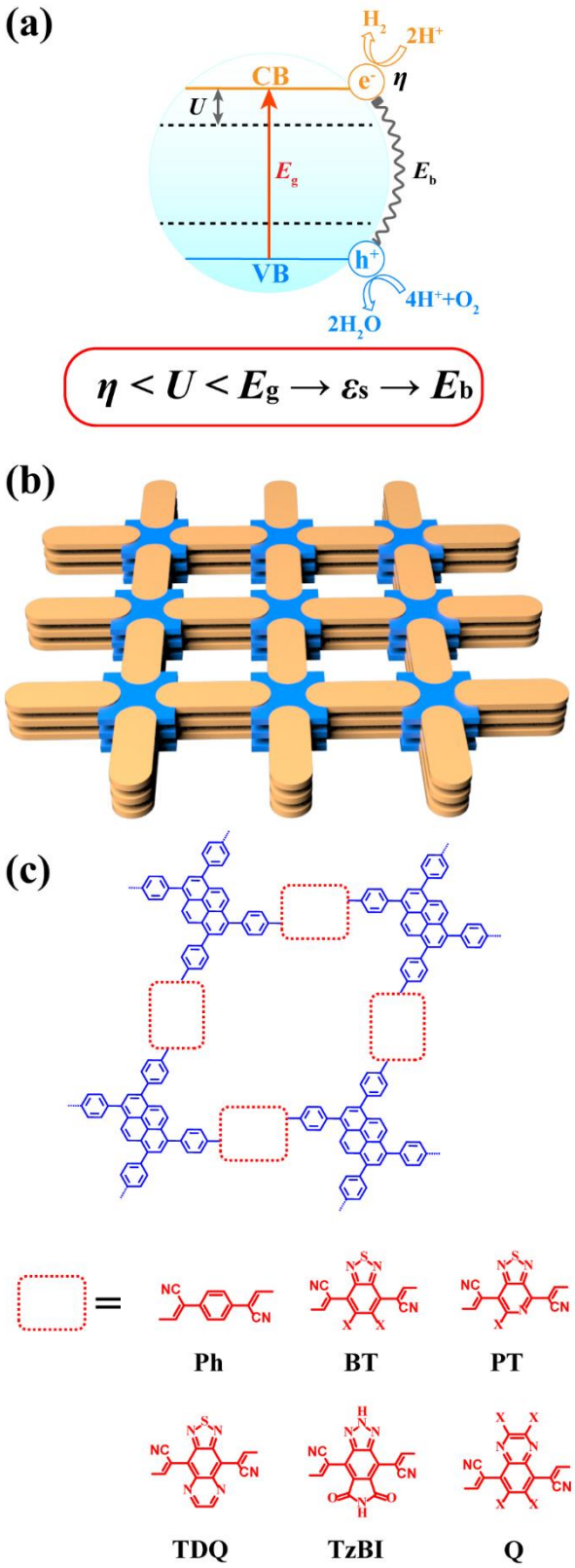

Fig. 1. (A) Schematic illustration of the inter-realtions between the overpotential (η), the driving force (U), the band gap (E_g), and the exciton binding energy (E_b). **(B)** Topological structure and building blocks of stacked 2D COFs of Lieb lattice with nodes highlighted in blue and edges in orange. **(C)** Chemical structures of PPy-Ph, PPy-BT, PPy-PT, PPy-TDQ, PPy-TzBI and PPy-Q. PPy represents the pyrene node

and it is short for tetrakis(4-formylphenyl)phenyl. Ph, BT, PT, TDQ, TzBI, and Q represent the edges, which are short for phenyl, benzothiadiazole, pyridal[2,1,3]thiadiazole, thiadiazolo-quinoxaline, pyrrolo[3,4-f]benzotriazole-5,7-dione, and quinoxaline, respectively. X = -H or -F.

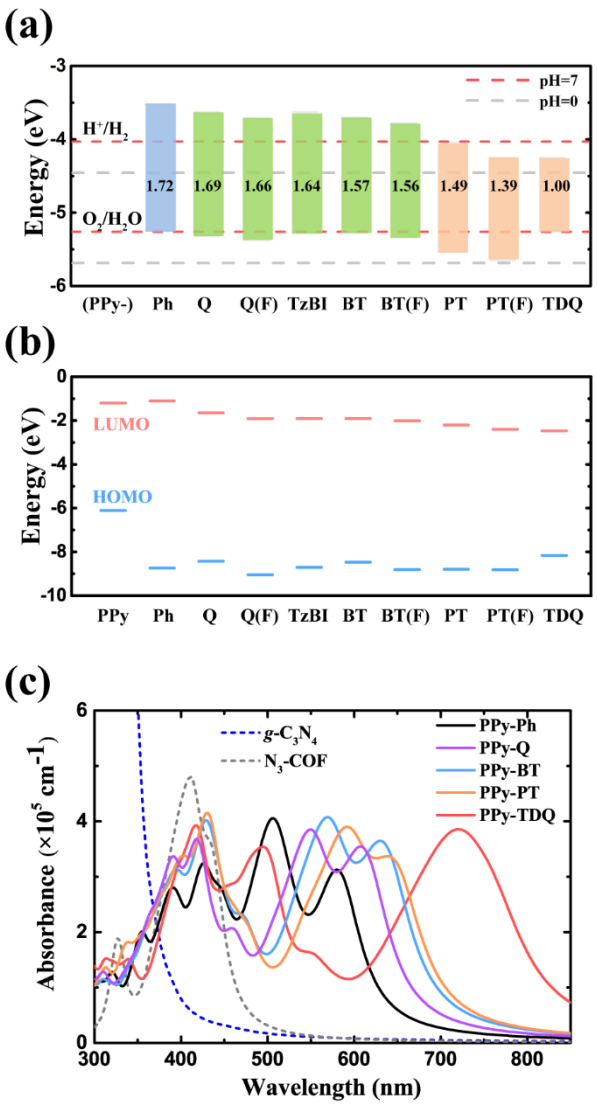

Fig. 2. (A) Energies of VBM and CBM in COFs relative to the vacuum level calculated with the HSE06 functional. The red and gray dashed lines represent redox potentials of water at pH = 7 and pH = 0, respectively. Band gaps are also shown in the figure. COFs capable of HER only, OER only and overall water splitting are shown in blue, orange and green, respectively. **(B)** HOMO and LUMO energy level diagram for molecular building blocks of COFs. PPy represents the pyrene node, and Ph, BT, BT(F), PT, PT(F), TDQ, TzBI, Q, and Q(F) represent edges of COFs. **(C)** Optical absorption spectra of PPy-Ph, PPy-BT, PPy-PT, PPy-TDQ, and PPy-Q in comparison to *g*-C_3N_4 and N_3-COF. All these spectra are calculated with G_0W_0-BSE method.

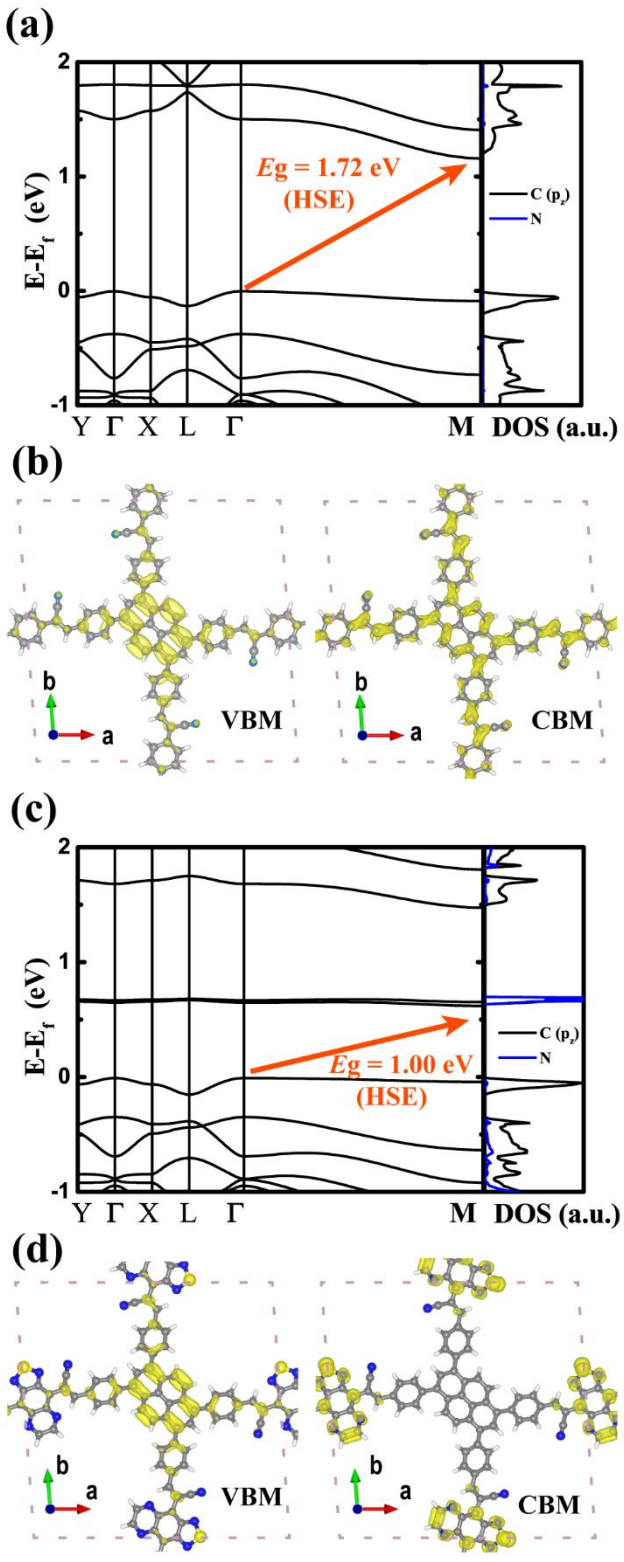

Fig. 3. (A) Band structure and partial density of states of PPh-Ph. **(B)** Charge density distribution at VBM and CBM of PPh-Ph. **(C)** Band structure and partial density of states of PPy-TDQ. **(D)** Charge density distribution at VBM and CBM of PPh-TDQ. Band structures are calculated with the PBE-D3 functional, and band gaps calculated with the HSE functional are provided in the figure. Spatially separated electron and hole in PPy-TDQ are demonstrated by charge density distribution at VBM and CBM.

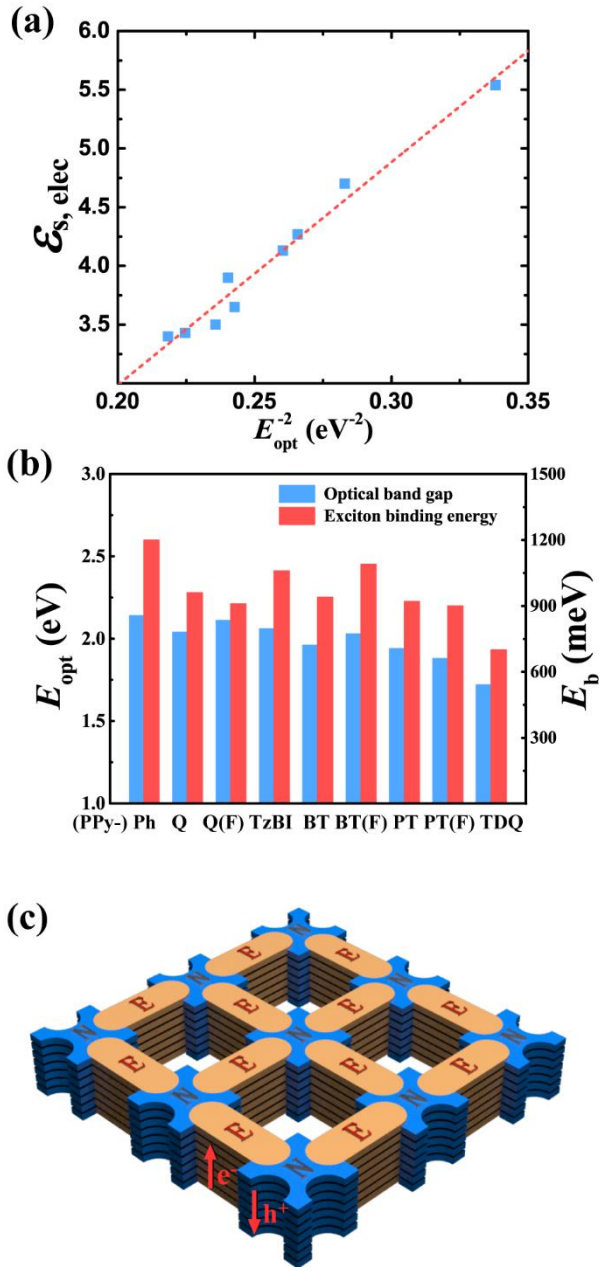

Fig. 4. (A) Relationship between the electronic static dielectric constant ($\varepsilon_{s,\,elec}$) and the optical band gap ($E_{opt} = \hbar\omega_e$) of COFs, well characterized by the formula $\varepsilon_{s,\,elec} = 1 + Ne^2/(m\varepsilon_0\omega_e^2)$. The red dashed line represents a linear fit of the data. **(B)** Positive correlation between the optical band gap and the exciton binding energy of COFs. **(C)** Schematic illustration of the out-of-plane stacked structure of COFs and the spatial separation of one-dimensional transport channels for electron and hole.

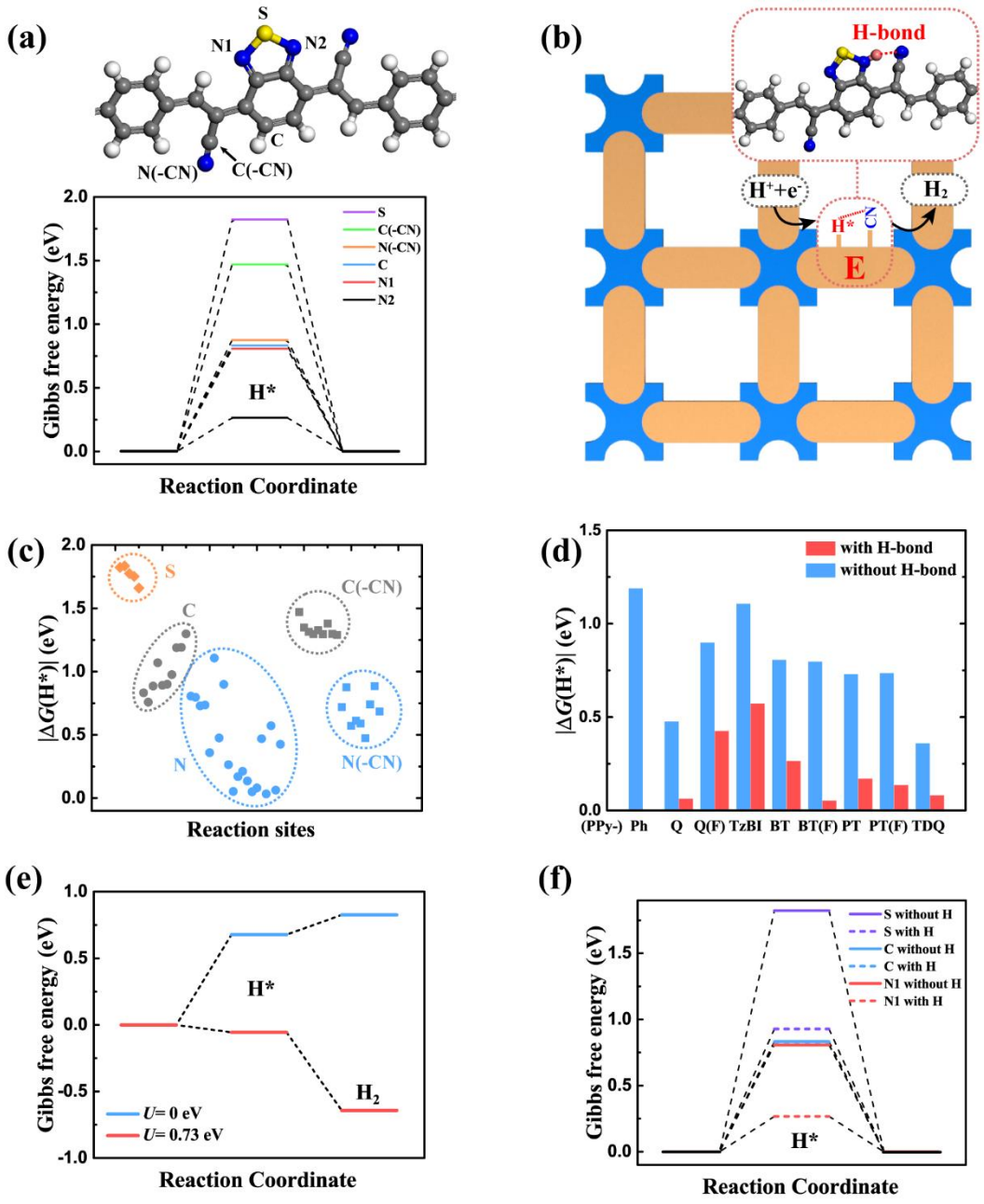

Fig. 5. (A) Gibbs free energy changes of metal-free HER process on different catalytic sites of PPy-BT at pH = 0. **(B)** Structural illustration of intermediate (H*) with hydrogen adsorption on the N2 site of PPy-BT and formation of a hydrogen bond with the nearby N(-CN). **(C)** Δ*G*(H*) for different types of reaction sites on the edge of all the COFs. **(D)** Δ*G*(H*) for the N1 and N2 sites on the edge of all the COFs, without and with hydrogen bond respectively. **(E)** Gibbs free energy changes of HER on the N2 site of PPy-BT at pH = 7 with *U* = 0 eV and *U* = 0.73 eV, respectively. **(F)** Gibbs free energy changes for different catalytic sites with or without hydrogen atom adsorption on the N2 site.

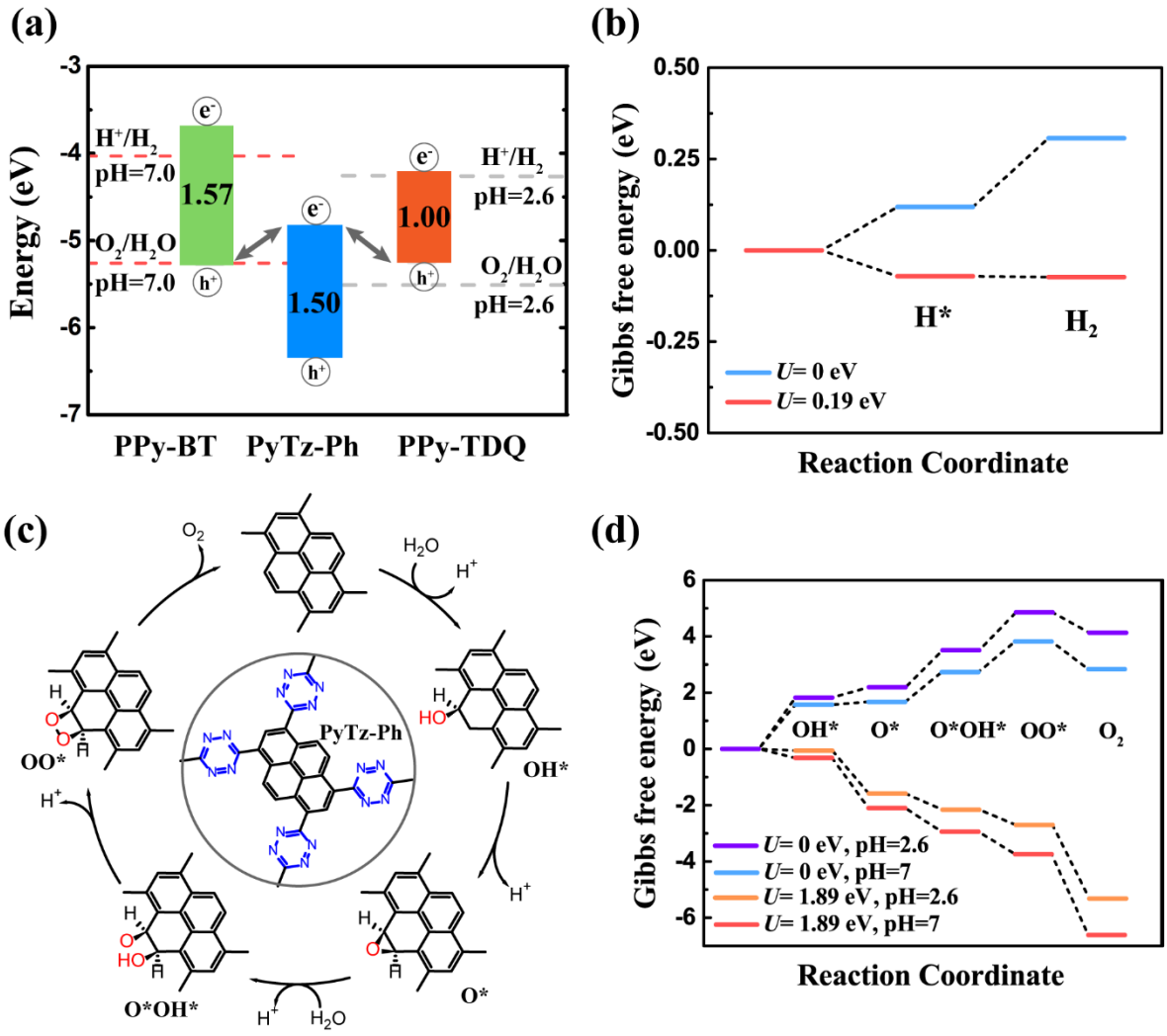

Fig. 6. (A) Band alignment of PPy-BT, PyTz-Ph, and PPy-TDQ in a direct Z-scheme system for overall water splitting. The red and gray dashed lines represent redox potentials of water at pH = 7 and pH = 2.6, respectively, corresponding to neutral solution and 0.1 M ascorbic acid solution. **(B)** Gibbs free energy changes of HER on the N3 site of PPy-TDQ at pH = 2.6 with U = 0 eV and U = 0.19 eV, respectively. **(C)** Illustration of OER processe on the PyTz unit of PyTz-Ph. **(D)** Gibbs free energy changes of OER on PyTz-Ph at pH = 7 and pH = 2.6 with U = 0 eV and U = 1.89 eV, respectively.

Table 1. Photoelectrochemical properties of designed COFs.

(Ppy-)	E_{opt} (eV)	$E_{g,}$ (eV)	U_{red} (eV)	$\|\eta_{HER}\|$ (eV)	$m^*_{exciton}$ /m_e	STH/ %	ε_s	E_b (meV)
Ph	2.14	1.72	0.92	0.72	0.21	27.8	3.60	1200
Q	2.04	1.69	0.81	0.06	0.26	28.8	4.22	960
Q(F)	2.11	1.66	0.73	0.43	0.29	29.7	4.65	910
TzBI	2.06	1.64	0.81	0.72	0.34	30.4	4.02	1060
BT	1.96	1.57	0.73	0.26	0.19	32.8	4.50	940
BT(F)	2.03	1.56	0.67	0.05	0.25	33.1	4.00	1090
PT	1.94	1.49	0.40	0.17	0.27	35.6	4.63	920
PT(F)	1.88	1.39	0.18	0.05	0.25	39.5	5.12	900
TDQ	1.72	1.00	0.19	0.03	0.29	56.6	6.05	700